Dissipative soliton resonances

W. Chang,[1] A. Ankiewicz,[1] J. M. Soto-Crespo,[2] and N. Akhmediev[1]
[1]*Optical Sciences Group, Research School of Physical Sciences and Engineering, The Australian National University, Canberra ACT 0200, Australia*
[2]*Instituto de Óptica, C.S.I.C., Serrano 121, 28006 Madrid, Spain*
(Received 2 April 2008; published 19 August 2008)

We have found a dissipative soliton resonance which applies to nonlinear dynamical systems governed by the complex cubic-quintic Ginzburg-Landau equation. Specifically, for particular values of the equation parameters, the soliton energy increases indefinitely. These equation parameters can easily be found using approximate methods, and the results agree very well with numerical ones. The phenomenon can be very useful in the design of high-power passively mode-locked lasers.

DOI: 10.1103/PhysRevA.78.023830 PACS number(s): 42.65.Tg, 42.65.Re

I. INTRODUCTION

The concept of the dissipative soliton has received wide recognition in optics, physics in general, biology, and medicine [1,2]. This concept allows many diverse phenomena in nature to be understood and studied in a simple and ordered way. It represents a unifying notion in science, since it stresses common features in a variety of complicated behaviors of self-localized formations. The most prominent feature of dissipative solitons is that they exist only when there is a continuous energy supply from an external source. This energy has to be dissipated in the medium where solitons are found. Thus their formation requires a balance between the energy supplied and lost. This balance must be exact in order to prevent the overheating or the cooling down of the system and the subsequent disappearance of the soliton. The exact balance is provided by the highly involved dynamics in the system, which implies that dissipative solitons have to be self-organized. Their shape, amplitude, width, and all other parameters are unique for given external conditions. Dissipative solitons can be natural, i.e., they can exist in nature as a result of a relaxation to a localized formation under the influence of solar heating and dissipation, or they can be artificial objects created by scientists. In the latter case, they can be used in modern technology.

Examples of dissipative solitons are [1,2] ultrashort pulses from passively mode-locked lasers, nerve pulses, localized formations in reaction-diffusion systems, vegetation clustering in arid lands, Bose-Einstein condensates in cold atoms, wave phenomena in neuron networks, spiral waves in weakly excitable media, and traveling waves in cortical networks [2]. This list is far from being complete. The variety of systems that admit dissipative solitons is enormous. The number of mathematical equations they satisfy is also very large. Nevertheless, they all have a common feature: they only "live" in the presence of a continuous energy supply from an external source. Thus they can be studied using certain common rules and principles.

One of the most important applications is the generation of ultrashort optical pulses with record-high energy [3]. Indeed, femtosecond optical pulses with extremely high energy provide modern experimental physics with new tools. Femtosecond laser oscillators with pulse energies in excess of 100 nJ and peak powers that exceed several megawatts [4,5] have the potential to replace more complex and expensive ultrashort pulse amplifier aggregates [6–9]. Applications include the generation of exceptionally wideband, or supercontinuum, light sources [10] that find numerous applications in biomedical imaging [11]. They can offer promising alternatives to the acceleration of charged particles [12]. They can be used for molecular finger printing [13], fabrication of optical couplers [14] and nanostructures in transparent dielectrics such as silica glass [15], high-density optical three-dimensional data storage [16], and high harmonic generation of attosecond pulses in the x-ray range [17]. Medical applications include accurate and precise laser surgery without destructive effects for the surrounding tissues [18], noninvasive manipulation of the structural machinery of cells and tissues [19], dissection of biological samples [20], accurate nondestructive dentistry [21], and delicate eye surgery [22]. The list of possible applications in all areas of human activity seems to be unlimited [23]. Thus producing shorter and more powerful pulses is vital for further progress in science and technology.

Until recently, the generation of ultrashort high-energy optical pulses required a cascade of delicate amplifiers at the output of a mode-locked oscillator. The technique is based on the concept of chirped-pulse amplification [24]. As a result, the required equipment increased dramatically in size and price. Recently, however, it was shown that high-energy pulses could be produced by a single solid-state laser [25], reducing the need for amplifiers. Fiber lasers have also been studied vigorously in this regard [26,27].

The large variety of cavity designs and the wide range of possible pulse dynamics prevents us from constructing a general theory of passively mode-locked lasers. Until recently, most scientific attention has been focused on cavity dispersion issues. Although soliton propagation in the anomalous dispersion regime can provide neat "*sech*-profile" pulses, the search for higher-energy and wider-bandwidth laser outputs has led to the design of cavities with strong dispersion management, featuring an average dispersion shifted into the normal regime [26–28]. The principle of dispersion management eventually evolved into the concepts of parabolic-pulse and all-normal-dispersion lasers [29]. The resulting stationary output pulses are usually strongly chirped, making them wider in the temporal domain, but further com-

pression outside the cavity can be used to shorten the pulses down to the femtosecond range.

One more theoretical step forward has been made in Ref. [3]. Namely, it was shown numerically that the energy of the dissipative solitons of the cubic-quintic complex Ginzburg-Landau (CGLE) increases significantly when its parameters are located on a special line in the space of parameters. It was also shown that the soliton spectra in this case resemble the three-peak spectra observed in the experimental results of Ref. [26]. Thus there is a strong connection between high energy generation by single optical oscillators and high energy solutions of the CGLE.

In the present work, we show that the soliton energy can increase indefinitely for certain values of the system parameters, and so the process resembles the resonance phenomenon in the theory of oscillators. Thus we call this phenomenon "dissipative soliton resonance." Using the method of moments, we have found an approximate relation between the parameters of the CGLE where the resonance manifests itself. The expression shows that the resonance appears mostly in the regime of normal dispersion, but can be shifted to the anomalous dispersion region by changing the system parameters.

II. COMPLEX GINZBURG-LANDAU EQUATION

Our approach is based on using the cubic-quintic Ginzburg-Landau equation [30,31] as the master equation [32] for modeling pulse generation by passively mode-locked lasers, including both solid-state [33] and fiber lasers [34]. Due to the large variety of laser designs [35], modeling each of them separately is a tedious task. It requires the use of several equations and we would need to take the particular cavity design into account. Using the master equation approach simplifies this work to some extent. It can be considered as a good approximation when the changes due to pulse evolution are relatively small during any individual round trip of the cavity. It allows us to find the critical parameters of the system that will generate the pulse with the highest possible energy. The model can be significantly improved by adding parameter-management techniques to the numerical simulations [36].

The cubic-quintic complex Ginzburg-Landau equation is given by [37]

$$i\psi_z + \frac{D}{2}\psi_{tt} + |\psi|^2\psi = -\nu|\psi|^4\psi + i\delta\psi + i\epsilon|\psi|^2\psi + i\beta\psi_{tt} + i\mu|\psi|^4\psi \equiv R[\psi], \tag{1}$$

where z is the propagation variable, t is the time in a frame that moves at the group velocity of the soliton, ψ is the normalized field envelope, D accounts for the dispersion, being positive (negative), in the anomalous (normal) dispersion regime, δ is the linear loss (if negative), ϵ is related to the nonlinear gain (if positive), and μ accounts for the nonlinear gain saturation (if negative). The term containing β controls the spectral filtering or gain dispersion (if positive) and ν accounts for the quintic nonlinearity. The terms on the right-hand side of Eq. (1) differentiate it from the nonlinear Schrödinger equation and are denoted by $R[\psi]$. This is done for convenience of notation in the equations that follow.

Equation (1) has a large number of localized solutions [38,39]. There are stationary [37,40], pulsating [41], exploding [42] and many other types of soliton solutions [41]. Transitions between them occur in the form of sequences of bifurcations. Because of such a plethora of different types of solutions, their classification is a difficult task. In the present work, we have found that the energy of some stationary solitons can take very large values when the system parameters enter a specific region. This phenomenon can be called "soliton resonance." In fact, the energy of the soliton may increase indefinitely at specific values of the system parameters, just as occurs with a resonance effect of a simple oscillator. We do not have a direct analytic technique that would allow us to find the resonance parameters using a straightforward procedure. This is related to the fact that analytic solutions of the CGLE are only known for very specific values of the parameters [37]. Instead, we use some approaches to predict the areas where resonances can be found, and later we confirm numerically that they do exist.

III. METHOD OF MOMENTS

Here we apply a technique called the method of moments [43] to approximate the stationary soliton solutions. In this method, we introduce five moments

$$Q = \int_{-\infty}^{\infty} |\psi|^2 dt,$$

$$P = \frac{1}{2}\int_{-\infty}^{\infty} (\psi\psi_t^* - \psi^*\psi_t) dt,$$

$$I_1 = \int_{-\infty}^{\infty} t|\psi|^2 dt, \tag{2}$$

$$I_2 = \int_{-\infty}^{\infty} (t - t_0)^2 |\psi|^2 dt,$$

$$I_3 = \int_{-\infty}^{\infty} (t - t_0)(\psi^*\psi_t - \psi\psi_t^*) dt, \tag{3}$$

which are conserved quantities of the nonlinear Schrödinger equation. For Eq. (1), they are not conserved but satisfy the following truncated set of first-order ordinary differential equations:

$$\frac{dQ}{dz} = i\int_{-\infty}^{\infty} (\psi R^* - \psi^* R) dt,$$

$$\frac{dP}{dz} = -i\int_{-\infty}^{\infty} (\psi_t R^* + \psi_t^* R) dt,$$

$$\frac{dI_1}{dz} = iDP + i\int_{-\infty}^{\infty} t(\psi R^* - \psi^* R) dt,$$

$$\frac{dI_2}{dz} = -iDI_3 + i\int_{-\infty}^{\infty}(t-t_0)^2(\psi R^* - \psi^* R)dt,$$

$$\frac{dI_3}{dz} = 2P\frac{dt_0}{dz} + i\int_{-\infty}^{\infty}(2D|\psi_t|^2 - |\psi|^4)dt + 2i\int_{-\infty}^{\infty}(t-t_0)$$
$$\times(\psi_t R^* + \psi_t^* R)dt + i\int_{-\infty}^{\infty}(\psi R^* + \psi^* R)dt. \quad (4)$$

The truncation is needed for the reduction of the number of degrees of freedom in order to simplify the problem. As a first step, we must select a trial function to approximate the stationary localized solution of the CGLE. After several attempts to find the most adequate trial function we have chosen the following higher-order Gaussian function:

$$\psi(t,z) = A\exp\left(-\frac{t^2}{w^2} - \frac{t^4}{4mw^4}\right)\exp(ict^2), \quad (5)$$

where A is the soliton amplitude, w is the soliton width, c is the soliton chirp, and m an adjustment parameter that we shall consider to be a constant. $A(z)$, $w(z)$, and $c(z)$ are variables that evolve along the propagation direction z. The arbitrary parameter m is a positive constant that adjusts the shape of the soliton. Generally, setting $4m=1$ gives good results over a wide range of the system parameters. Setting $4m$ to be smaller than 1 gives pulses which are closer to being rectangular. This improves the results slightly when the soliton energy becomes very large. However, the differences in the final results are very small over the whole interval where $m<1/4$. Thus we mainly use $4m=1$ in the rest of this work.

The equations for the moments for arbitrary positive real m are presented in Appendix A. When $4m=1$ the moments are

$$Q = 1.051A^2w, \quad I_2 = 0.145Qw^2, \quad I_3 = 4icI_2. \quad (6)$$

Our trial function is symmetric, so $P=0$ and $I_1=0$. The coefficients here are written with an accuracy of four digits. Then the evolution equations for the soliton parameters become

$$Q_z = Q\left(2\delta - \frac{3.738\beta}{w^2} - 1.158c^2w^2\beta + \frac{1.433Q\epsilon}{w} + \frac{1.146Q^2\mu}{w^2}\right),$$

$$w_z = w\left(2cD + \frac{2.142\beta}{w^2} - 0.874c^2w^2\beta - \frac{0.290Q\epsilon}{w} - \frac{0.325Q^2\mu}{w^2}\right),$$

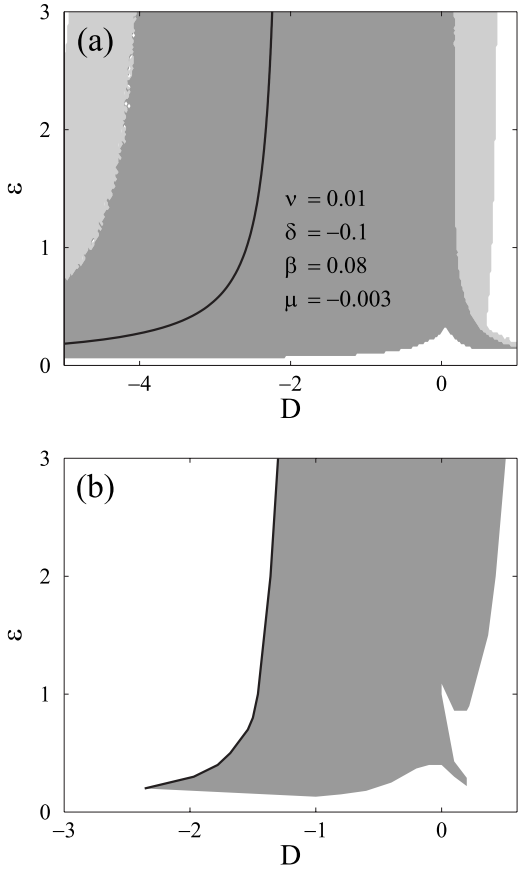

FIG. 1. (a) Region of existence of stable fixed points for the dynamical system given by Eq. (7) (dark shade) in the (D,ϵ) plane. The soliton energy Q and the width w increase to infinitely large values near the resonance curve shown in the middle by a solid line. (b) Numerical simulations of the CGLE from Ref. [3]. The approximation based on Eq. (7) is in reasonably good qualitative agreement with numerical simulations, apart from the fact that the stable soliton solutions are only found on the right-hand side of the resonance curve in the simulations. Consequently, the resonance curve (black) is the left-hand side border of the gray region containing stable solitons. The light gray region on the right-hand side of plot (a) corresponds to periodic solutions. These are pulsating solitons, also found in numerical simulations [3] but not shown here in (b).

$$c_z = \frac{1}{w^2}\left(-2c^2w^2D + \frac{6.453D}{w^2} - \frac{1.237Q}{w} - \frac{1.319Q^2\nu}{w^2} - 19.624c\beta\right). \quad (7)$$

The dynamical system Eq. (7) has a relatively simple structure. The right-hand sides of the three equations are rational expressions of Q, w, and c. Using standard techniques, we can find its fixed points and study their stability. The results for fixed values of δ, ν, β, and μ are shown in Fig. 1(a). The dark gray region consists of stable fixed points, while the light gray region corresponds to oscillating solutions (limit cycles). The black curve in the middle is the resonance curve where energy Q increases to infinitely large values.

The shape and position of the resonance curve are in reasonably good agreement with the exact curve found numeri-

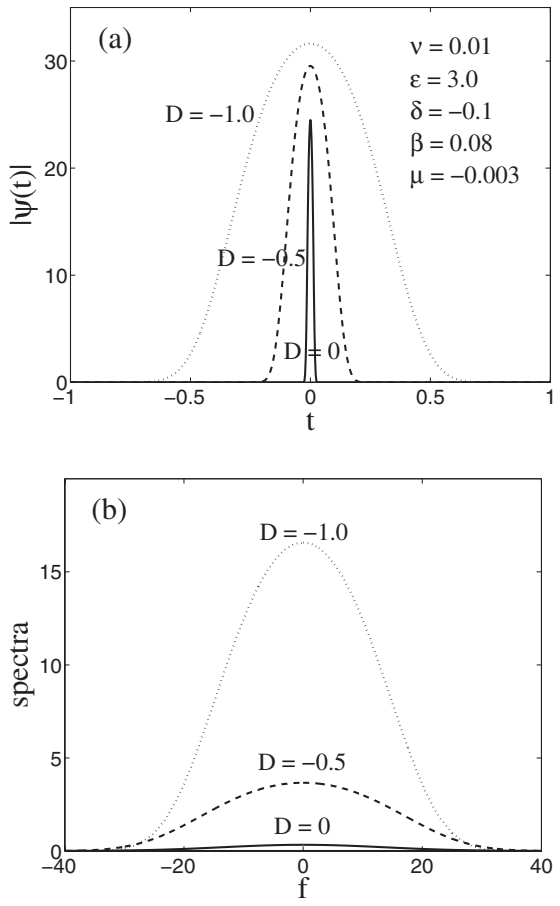

FIG. 2. (a) Reduced model pulse profiles and (b) soliton spectra for the set of parameters shown inside the plots. The qualitative changes in both the profiles and the spectra as D is varied agree well with those of the exact soliton solutions in Ref. [3].

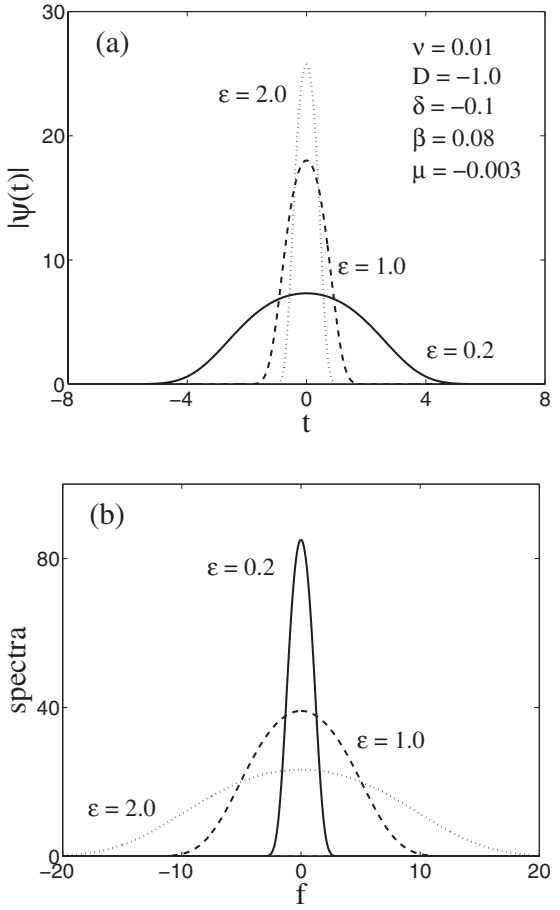

FIG. 3. (a) Reduced model pulse profiles and (b) soliton spectra for the set of parameters shown inside the figures. The qualitative changes, in both the profiles and the spectra, as ϵ is varied agree well with those of the exact soliton solutions in Ref. [3].

cally in [3]. Figure 1(b) is taken from [3]. The shape of the region on the right-hand side of the resonance curve is also in good agreement with the numerical results. Even fine features like the little "hamster tail" in the right bottom corner of the plot is well-reproduced by the trial function approximation. Moreover, oscillating solutions, that correspond to pulsating solitons in numerical simulations, also appear and are depicted by the light gray region on the right-hand side of the plot. However, the region to the left of the resonance curve seems to be an artifact of the method. We have checked using numerical simulations of the CGLE that stable soliton solutions do not exist to the left of the resonance curve. This could be related to the fact that, in the infinite-dimensional dynamical system, more possibilities for instability appear, but these may be lost in a simple three-dimensional approximation [such as that given by Eq. (7)].

Using the soliton parameters obtained as fixed points of the dynamical system, Eq. (7), we can reconstruct the soliton profiles and their spectra. The results of this reconstruction are shown in Fig. 2. Starting from the value $D=0$ and approaching the resonance curve, we observe that the soliton width and amplitude increase [see Fig. 2(a)]. However, the amplitude increases slowly and its maximum value is restricted due to the saturation related to negative μ. Thus the energy Q close to the resonance increases mainly due to the increase of the pulse width. Clearly, to obtain high-energy ultrashort pulses, a linear pulse compression technique has to be used outside the cavity.

The soliton spectra also increase in strength, as we see from Fig. 2(b). These observations are in qualitatively good agreement with the numerical simulations of CGLE (see Fig. 2. of Ref. [3]). However, the exact spectra differ in shape. The simple trial function Eq. (5) cannot reproduce the additional side peaks. The real chirp is more complicated than a quadratic function of t.

The fact that the pulse width increases while its spectrum does not become narrower appears to contradict Fourier transform rules. However, the pulses here are not transform limited. They are chirped and this allows for the observed growth of the width without any corresponding compression of the pulse spectra. On approaching the resonance, the chirp, c, approaches zero, but the Fourier integral is over an ever-widening range. Simple analytic calculations (see Appendix C) show that these factors compensate, and, as a result, the spectral width approaches a constant.

We can also reproduce the soliton shapes and spectra when varying ϵ. These data are shown in Fig. 3. Both soliton profiles and spectra are in good qualitative agreement with the numerical results shown in Fig. 3 of [3], except for the

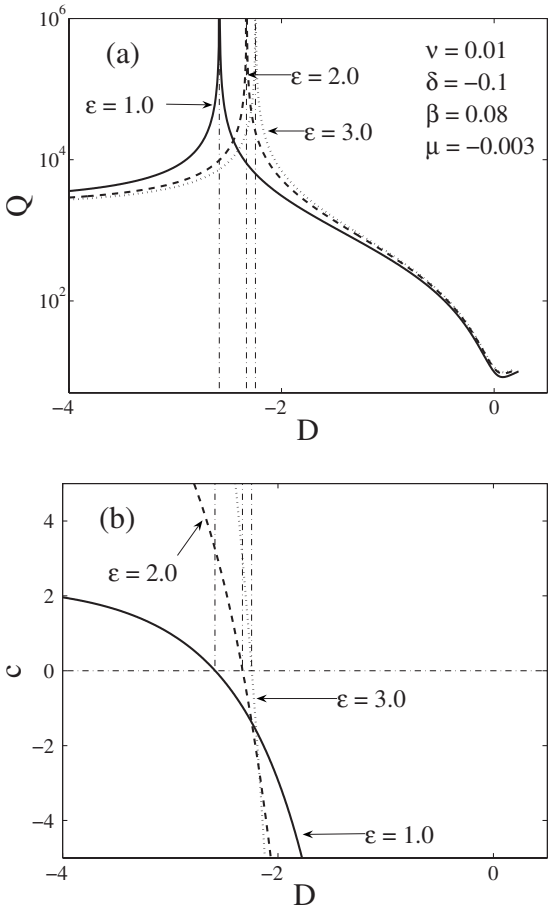

FIG. 4. (a) Soliton energy Q vs dispersion parameter D for three ϵ values in the generalized Gaussian model with $4m=1$. In the exact simulations, the fixed soliton curves on the left-hand side of the asymptotes do not appear. They would not be observed in experiments and may represent unstable solitons. (b) Chirp parameter c vs D for the same simulations. Vertical lines show that the chirp parameter is zero at resonance.

additional side maxima in the spectra. These are again related to the differences in chirps between the numerical results and the simple approximation Eq. (5).

To demonstrate the existence of the resonance phenomenon, we plot the soliton energy as a function of D in Fig. 4(a), for three different values of ϵ. For each ϵ, the corresponding curve shows clearly that the energy grows indefinitely as we approach a fixed D value from either side. If we ignore the parts of the curves on the left-hand side of the resonance, then the remaining part of the curve is in excellent qualitative agreement with the numerical results shown in Fig. 4 of [3]. Moreover, our approximation shows the existence of the resonance more clearly, since these curves can be plotted to very high values of Q. In the present plots, we have extended them up to the value of $Q \approx 10^6$. Reaching such values in the simulations of the CGLE may produce numerical artifacts due to sampling difficulties.

IV. RESONANCE CURVE

One of the main advantages of the present approximation is that the resonance curve can be found analytically. Near the resonance curve, the soliton parameters have the following asymptotic behavior: $Q \to \infty$, $w \to \infty$, and $c \to 0$. When nearing the resonance, the values Q/w and cw tend to approach constants with chirp c being negative. Using these observations, we can derive an analytic expression for the resonance curve in terms of the system parameters. Detailed calculations for a general m value are presented in Appendix D. For the generalized Gaussian case with $4m=1$, we obtain:

$$\frac{Q}{w} = -\frac{0.363k}{\mu},$$

$$cw = -\sqrt{\frac{0.472\delta\mu - 0.035k\epsilon}{\beta\mu}}, \tag{8}$$

where

$$k = 1.588\epsilon + \sqrt{2.522\epsilon^2 - 9.632\delta\mu}. \tag{9}$$

Then, the equation for the resonance curve takes the form

$$D = \frac{k\beta(0.330k\nu - 0.853\mu)}{\mu(0.135k\epsilon - 1.793\delta\mu)}. \tag{10}$$

For the set of system parameters used in Fig. 1(a), the term containing 2δ in the first of Eq. (7) is very small in comparison with the other terms. Thus we can neglect the 2δ term and obtain much simpler expressions for Q/w, cw, and the resonance curve. We find

$$\frac{Q}{w} = -\frac{1.152\epsilon}{\mu}(>0),$$

$$cw = -0.336\frac{\epsilon}{\sqrt{-\beta\mu}}(<0). \tag{11}$$

Then the equation for the resonance curve becomes

$$D = \left(\frac{7.778\nu}{\mu} - \frac{6.333}{\epsilon}\right)\beta. \tag{12}$$

Near the resonance, the soliton increases its width indefinitely while keeping its amplitude constant. Indeed, from the first of Eq. (6), we can see that the central intensity, A^2, is about $-1.1\epsilon/\mu$, i.e., it remains fixed. The amplitude of this wide soliton is $A \approx \sqrt{-\epsilon/\mu}$. It remains constant as the width, and hence energy, approach high values.

The black resonance curve in Fig. 1(a) is very well-approximated by Eq. (12). Qualitatively, it has the same features as the resonance curve obtained from the numerical simulations of CGLE [3], apart from a horizontal shift to the left along the D axis. Thus we can select coefficients in Eq. (12) and shift the curve to describe the exact resonance one. Adjusting one of the coefficients in Eq. (12) as follows:

$$D = \left(\frac{3.8\nu}{\mu} - \frac{6.333}{\epsilon}\right)\beta, \tag{13}$$

allows us to obtain virtually the exact curve presented in Fig. 1 of Ref. [3]. As we require, Eq. (13) is simply a lateral translation of the curve given by Eq. (12) to more positive values of D.

One of the important physical conclusions from the above calculations is that the resonance phenomenon occurs continuously along a surface in the six-dimensional space of equation parameters, and is not restricted to a particular point. The resonance curve that we have presented in Fig. 1(a) is merely a section of this surface in the plane of parameters D and ϵ. This means that the resonance can be found over a wide range of parameters of the system. When dealing with passively mode-locked lasers of virtually any design, we can find the resonance by choosing the cavity parameters from a broad range of values.

In the experimental setups of the works [25,26,44], the cavity dispersion was chosen to be normal (negative D). From a physical point of view, this choice was dictated by the evolution of knowledge in chirped pulse oscillators [44]. Our present results show that this choice is not an overall restriction for high energy soliton generation by a single optical oscillator. The point of resonance can be moved along the surface by changing the parameters of the system. In particular, the resonance curve can be moved towards regions with positive D. For example, this can occur when ν and μ are both negative. From Eq. (12), we then need the condition

$$\frac{\nu}{\mu} > \frac{0.814}{\epsilon} \tag{14}$$

for D to be positive. This simple consideration shows that we do not necessarily have to make a cavity with normal dispersion in order to build single oscillators that generate high energy pulses.

V. CONCLUSIONS

In conclusion, we have presented a simple trial function approximation for the phenomenon of dissipative soliton resonance found earlier using numerical simulations of the cubic-quintic complex Ginzburg-Landau equation. We have found a simple analytic expression for the resonance curve which is in good qualitative agreement with the results of numerical simulations. This expression shows that the resonance mainly occurs in the region of normal dispersion (negative D), but can be shifted to the region of anomalous dispersion by changing other parameters of the CGLE. Various expressions for the trial function are given that allow us to obtain better approximations for the resonance curve and the basic soliton parameters.

These results can be useful in constructing passively mode-locked laser systems that generate record-high energy pulses out of single oscillators, without the need for additional amplifiers.

ACKNOWLEDGMENTS

This research was supported under Australian Research Council's Discovery Projects funding scheme (Project No. DP0663216). The work of J.M.S.C. was supported by the M.E.y C. under Contract No. FIS2006-03376.

APPENDIX A: EQUATIONS FOR THE DYNAMICAL SYSTEM

In this appendix, we provide the general equations for the three-dimensional dynamical system generated by the trial function given by Eq. (5) with arbitrary real constant m. First, the moments are defined by

$$Q = \sqrt{m}e^m K_{1/4}(m) A^2 w,$$

$$I_2 = m\left(\frac{K_{3/4}(m)}{K_{1/4}(m)} - 1\right) Q w^2,$$

$$I_3 = 4icI_2, \tag{A1}$$

where $K_p(r)$ is the modified Bessel function of order p and argument r.

The dynamical system for the evolution of the soliton energy, Q, width w, and quadratic chirp coefficient c is given by

$$Q_z = Q\left(2\delta + s_1\frac{\beta}{w^2} + s_2 c^2 w^2 \beta + s_3\frac{Q\epsilon}{w} + s_4\frac{Q^2\mu}{w^2}\right),$$

$$w_z = w\left(2cD + r_1\frac{\beta}{w^2} + r_2 c^2 w^2 \beta + r_3\frac{Q\epsilon}{w} + r_4\frac{Q^2\mu}{w^2}\right),$$

$$c_z = \frac{1}{w^2}\left(-2c^2 w^2 D - v_1\frac{D}{w^2} - v_2\frac{Q}{w} - v_3\frac{Q^2\nu}{w^2} + v_4 c\beta\right). \tag{A2}$$

The coefficients in the above equations are given in analytical form:

$$s_1 = 1 - \frac{3K_{3/4}(m)}{K_{1/4}(m)}, \quad s_2 = 8m - \frac{8mK_{3/4}(m)}{K_{1/4}(m)},$$

$$s_3 = \frac{2K_{1/4}(2m)}{\sqrt{m}K_{1/4}^2(m)}, \quad s_4 = \frac{2K_{1/4}(3m)}{mK_{1/4}^3(m)}, \tag{A3}$$

and

$$r_1 = \frac{-4(3+m)(-1+2m)K_{1/4}^2(m)}{4mK_{1/4}(m)[K_{1/4}(m) - K_{3/4}(m)]} + \frac{mK_{1/4}(m)r_{1b} + mK_{3/4}(m)r_{1c}}{4mK_{1/4}(m)[K_{1/4}(m) - K_{3/4}(m)]},$$

$$r_2 = \frac{2\cdot 2^{3/4}e^{-m}m^{1/4}K_{3/4}(m)r_{2b} + K_{1/4}(m)r_{2c}}{K_{1/4}^2(m) - K_{1/4}(m)K_{3/4}(m)},$$

$$r_3 = \frac{K_{1/4}(2m)K_{3/4}(m) - K_{1/4}(m)K_{3/4}(2m)}{\sqrt{m}K_{1/4}^2(m)[K_{1/4}(m) - K_{3/4}(m)]},$$

$$r_4 = \frac{K_{1/4}(3m)K_{3/4}(m) - K_{1/4}(m)K_{3/4}(3m)}{mK_{1/4}^4(m) - mK_{1/4}^3(m)K_{3/4}(m)}, \tag{A4}$$

where

$$r_{1b} = 2(5-28m)K_{3/4}(m) + 2(26m-11)K_{5/4}(m) + 8mK_{7/4}(m),$$

$$r_{1c} = 4mK_{7/4}(m) - 12K_{3/4}(m),$$

$$r_{2b} = 2\sqrt{2m}\Gamma\left(\frac{5}{4}\right)H\left(\frac{5}{4},\frac{3}{2},2m\right) - \Gamma\left(\frac{3}{4}\right)H\left(\frac{3}{4},\frac{1}{2},2m\right),$$

$$r_{2c} = 4(1+m)K_{1/4}(m) - 4mK_{5/4}(m). \tag{A5}$$

The function $H(i,j,k)$ in Eq. (A5) is the hypergeometric function $({}_1F_1)$ with arguments (i,j,k) while $\Gamma(r)$ is the Euler gamma function.

Finally, the coefficients v_i are defined by

$$v_1 = -\frac{K_{1/4}(m) - 3K_{3/4}(m)}{4mK_{1/4}(m) - 4mK_{3/4}(m)},$$

$$v_2 = -\frac{K_{1/4}(2m)}{m^{3/2}[4K_{1/4}^2(m) - 4K_{1/4}(m)K_{3/4}(m)]},$$

$$v_3 = \frac{K_{1/4}(3m)}{3m^2K_{1/4}^2(m)[-K_{1/4}(m) + K_{3/4}(m)]},$$

$$v_4 = \frac{(-1+8m)K_{1/4}(m)}{m[K_{1/4}(m) - K_{3/4}(m)]} + \frac{2m[-9K_{3/4}(m) + 5K_{5/4}(m)]}{m[K_{1/4}(m) - K_{3/4}(m)]}. \tag{A6}$$

All equations above are valid for arbitrary real positive constant m. For each m, the coefficients can be calculated and given their arithmetic values. This has been done for $m = 1/4$ in the main text of the paper.

APPENDIX B: RESONANCE CURVE

Near the resonance curve, $Q \to \infty$, $w \to \infty$, and $c \to 0$. The terms of the order of c and w^{-2} in Eq. (A2) are close to zero and can be neglected. The dynamical system is then simplified and takes the form

$$Q_z = Q\left(2\delta + s_2c^2w^2\beta + s_3\frac{Q\epsilon}{w} + s_4\frac{Q^2\mu}{w^2}\right),$$

$$w_z = w\left(r_2c^2w^2\beta + r_3\frac{Q\epsilon}{w} + r_4\frac{Q^2\mu}{w^2}\right),$$

$$c_z = \frac{1}{w^2}\left(-2c^2w^2D - v_2\frac{Q}{w} - v_3\frac{Q^2\nu}{w^2}\right), \tag{B1}$$

where the coefficients s_i, r_i, and v_i are given by Eqs. (A3), (A4), and (A6), respectively.

The fixed points near the resonance curve are defined by the zeros of the right-hand side of Eq. (B1):

$$\left(2\delta + s_2c^2w^2\beta + s_3\frac{Q\epsilon}{w} + s_4\frac{Q^2\mu}{w^2}\right) = 0,$$

$$\left(r_2c^2w^2\beta + r_3\frac{Q\epsilon}{w} + r_4\frac{Q^2\mu}{w^2}\right) = 0,$$

$$\left(2c^2w^2D + v_2\frac{Q}{w} + v_3\frac{Q^2\nu}{w^2}\right) = 0. \tag{B2}$$

Near the resonance curve, the values Q/w and cw approach constants. Solving the first two equations in Eq. (B2) relative to Q/w and cw, we obtain:

$$\frac{Q}{w} = \frac{k}{2(r_2s_4 - r_4s_2)\mu},$$

$$cw = -\sqrt{\frac{k(r_4s_3 - r_3s_4)\epsilon + 4r_4(r_2s_4 - r_4s_2)\delta\mu}{2(r_4s_2 - r_2s_4)^2\beta\mu}}, \tag{B3}$$

where

$$k = \epsilon(r_3s_2 - r_2s_3) + \sqrt{(r_3s_2 - r_2s_3)^2\epsilon^2 + 8r_2(r_4s_2 - r_2s_4)\delta\mu}. \tag{B4}$$

Now we substitute Eq. (B3) into the third equation in Eq. (B2) and obtain the expression for the resonance curve in terms of the system parameters:

$$D = \frac{k\beta[2(r_2s_4 - r_4s_2)v_2\mu + kv_3\nu]}{4\mu[k(r_3s_4 - r_4s_3)\epsilon + 4r_4(r_4s_2 - r_2s_4)\delta\mu]}. \tag{B5}$$

The term containing 2δ in Eq. (B2) is much smaller than the other terms for the set of parameters that we use in numerical simulations. Neglecting it, we can obtain a much simpler equation for the resonance curve. Following the same procedures as above, we find

$$\frac{Q}{w} = \frac{(r_2s_3 - r_3s_2)\epsilon}{(r_4s_2 - r_2s_4)\mu},$$

$$cw = -\sqrt{\frac{(r_3s_2 - r_2s_3)(r_4s_3 - r_3s_4)\epsilon^2}{(r_4s_2 - r_2s_4)^2\beta\mu}}. \tag{B6}$$

Then the expression for the resonance curve becomes

$$D = \frac{(r_4s_2 - r_2s_4)v_2\beta\mu + (r_2s_3 - r_3s_2)v_3\beta\epsilon\nu}{2(r_4s_3 - r_3s_4)\epsilon\mu}. \tag{B7}$$

APPENDIX C: FINITE SPECTRAL WIDTH NEAR THE RESONANCE

For a pulse with constant amplitude A, and width w, we can readily estimate the width of the spectrum for the basic model as we approach the high-Q line where the width becomes infinite. The Fourier transform is defined as

$$F(\omega) = \frac{A}{\sqrt{2\pi}}\int_{-w/2}^{w/2}\exp(ict^2 + i\omega t)dt,$$

with chirp $c = -r/w$ and constant r, as explained earlier. Hence

$$|F(\omega)| = \frac{A}{2}\sqrt{\frac{w}{2r}}|\mathrm{erf}(g_-) + \mathrm{erf}(g_+)|,$$

where the arguments of the error functions, erf, are given by

$$g_\pm = \frac{1}{2}(-1)^{1/4}\sqrt{\frac{w}{r}}(r \pm \omega).$$

So, in taking the limit as $w \to \infty$, we obtain

$$|F(\omega)| = A\sqrt{\frac{w}{2r}} \quad \text{if } \omega^2 < r^2,$$

and zero if $\omega^2 > r^2$.

The total energy $[\approx \int_{-r}^{r} |F(\omega)|^2 d\omega]$, is then clearly proportional to the width, w, while the spectral width is fixed at $2r$. Thus the presence of chirp means that we do not get a very narrow spectral width near the high-Q line, whereas we would expect a very narrow spectrum for a transform limited pulse. Even for cases with Gaussian amplitude, which are thus not close to the resonance, the spectrum remains roughly of constant width as the pulse width increases.

APPENDIX D: QUARTIC TRIAL FUNCTION

We now consider a new trial function. It is related to the one in the main text, but is not a limiting case of it. This trial function involves only the quartic term:

$$\psi(t,z) = A\exp\left(-\frac{t^4}{w^4}\right)\exp(ict^2). \tag{D1}$$

Equation (D1) gives a slightly better approximation of the soliton characteristics when the soliton energy reaches extremely high values. However, the differences are not very dramatic. For the sake of completeness, we give the main equations in this appendix.

When we use the quartic trial function, i.e., Eq. (D1), then the moments are given by the following expressions:

$$Q = 2^{3/4}\Gamma\left(\frac{5}{4}\right)A^2 w,$$

$$I_2 = \frac{\Gamma\left(\frac{3}{4}\right)}{\sqrt{2}\Gamma\left(\frac{1}{4}\right)}Qw^2, \quad I_3 = 4icI_2. \tag{D2}$$

The dynamical system is described by the same three coupled ordinary differential equations of Eq. (A2) except for the coefficients that take the following particular forms:

$$s_1 = -\frac{12\pi}{\Gamma^2\left(\frac{1}{4}\right)}, \quad s_2 = -\frac{8\pi}{\Gamma^2\left(\frac{1}{4}\right)},$$

$$s_3 = \frac{4}{\Gamma\left(\frac{1}{4}\right)}, \quad s_4 = \frac{8\sqrt{2}}{3^{1/4}\Gamma^2\left(\frac{1}{4}\right)}, \tag{D3}$$

while the coefficients r_i are given by

$$r_1 = \frac{6\pi}{\Gamma^2\left(\frac{1}{4}\right)} - \frac{\Gamma^2\left(\frac{1}{4}\right)}{4\pi}, \quad r_2 = \frac{4\pi}{\Gamma^2\left(\frac{1}{4}\right)} - \frac{\Gamma^2\left(\frac{1}{4}\right)}{2\pi},$$

$$r_3 = \frac{-2+\sqrt{2}}{\Gamma\left(\frac{1}{4}\right)}, \quad r_4 = -\frac{8\sqrt{-3+2\sqrt{3}}}{3\Gamma^2\left(\frac{1}{4}\right)}, \tag{D4}$$

and for v_i, we have

$$v_1 = -3, \quad v_2 = \frac{\Gamma\left(\frac{1}{4}\right)}{2\pi},$$

$$v_3 = \frac{4\sqrt{2}}{3\cdot 3^{1/4}\pi}, \quad v_4 = -\frac{4\Gamma^2\left(\frac{1}{4}\right)}{\pi}. \tag{D5}$$

The expression for the resonance curve is the same as that in the previous section with the coefficients given by Eqs. (D3)–(D5).

On neglecting the 2δ term in the dynamical system, we find, for the two constants:

$$\frac{Q}{w} = -\frac{1.155\epsilon}{\mu} \quad (>0),$$

$$cw = -0.269\frac{\epsilon}{\sqrt{-\beta\mu}} \quad (<0). \tag{D6}$$

In this case, the resonance curve takes the form

$$D = \left(\frac{7.611\nu}{\mu} - \frac{6.208}{\epsilon}\right)\beta, \tag{D7}$$

which is slightly closer to the exact curve than Eq. (12). This is because Eq. (D1) provides fairly rectangular pulses which match better the actual pulses near the resonance.

[1] *Dissipative Solitons*, edited by N. Akhmediev and A. Ankiewicz, Lecture Notes in Physics, Vol. 661 (Springer, Berlin, 2005).

[2] *Dissipative Solitons: From Optics to Biology and Medicine*, edited by N. Akhmediev and A. Ankiewicz, Lecture Notes in Physics, Vol. 751 (Springer, Berlin, 2008).

[3] N. Akhmediev, J. M. Soto-Crespo, and Ph. Grelu, Phys. Lett. A **372**, 3124 (2008).

[4] S. H. Cho, F. X. Kärtner, U. Morgner, E. P. Ippen, J. G. Fujimoto, J. E. Cunnighan, and W. H. Knox, Opt. Lett. **26**, 560 (2001).

[5] A. M. Kowalevicz, Jr., A. T. Zare, F. X. Kärtner, J. G. Fujimoto, S. Dewald, U. Morgner, V. Scheuer, and G. Angelow, Opt. Lett. **28**, 1597 (2003).

[6] S. Backus, R. Bartels, S. Thompson, R. Dollinger, H. C. Kapteyn, and M. M. Murnane, Opt. Lett. **26**, 465 (2001).

[7] Y. Jiang, T. Lee, W. Li, G. Ketwaroo, and Ch. G. Rose-Petruck, Opt. Lett. **27**, 963 (2002).

[8] J. Seres, A. Müller, E. Seres, K. O'Keeffe, M. Lenner, R. F. Herzog, D. Kaplan, Ch. Spielmann, and F. Krausz, Opt. Lett. **28**, 1832 (2003).
[9] R. Huber, F. Adler, A. Leitenstorfer, M. Beutter, P. Baum, and E. Riedle, Opt. Lett. **28**, 2118 (2003).
[10] G. Genty, S. Coen, and J. M. Dudley, J. Opt. Soc. Am. B **24**, 1771 (2007).
[11] N. Nishizawa, Y. Chen, P. Hsiung, E. P. Ippen, and J. G. Fujimoto, Opt. Lett. **29**, 2846 (2004).
[12] M. Kando *et al.*, Jpn. J. Appl. Phys., Part 2 **38**, L967 (1999).
[13] S. A. Diddams, L. Hollberg, and V. Mbele, Nature (London) **445**, 627 (2007).
[14] K. Suzuki, V. Sharma, J. G. Fujimoto, and E. P. Ippen, Opt. Express **14**, 2335 (2006).
[15] R. S. Taylor, C. Hnatovsky, E. Simova, D. M. Rayner, V. R. Bhardwaj, and P. B. Corkum, Opt. Lett. **28**, 1043 (2003).
[16] G. Cheng, Y. Wang, J. D. White, Q. Liu, W. Zhao, and G. Chen, J. Appl. Phys. **94**, 1304 (2003).
[17] I. P. Christov, M. M. Murnane, and H. C. Kapteyn, Phys. Rev. Lett. **78**, 1251 (1997).
[18] K. König, O. Krauss, and I. Riemann, Opt. Express **10**, 171 (2002).
[19] I. Maxwell, S. Chung, and E. Mazur, Med. Laser Appl. **20**, 193 (2005).
[20] M. Sakakura, S. Kajiyama, M. Tsutsumi, J. Si, E. Fukusaki, Y. Tamaru, S. Akiyama, K. Miura, K. Hirao, and M. Ueda, Jpn. J. Appl. Phys., Part 1 **46**, 5859 (2007).
[21] J. Serbin, T. Bauer, C. Fallnich, A. Kasenbacher and W. H. Arnold, Appl. Surf. Sci. **197-198**, 737 (2002).
[22] B. G. Wang, I. Riemann, H. Schubert, K. J. Halbhuber, and K. Koenig, Cell Tissue Res. **328**, 515 (2007).
[23] F. Dausinger, RIKEN Review No. 43, 2002 (unpublished), pp. 8–13.
[24] D. Strickland and G. Mourou, Opt. Commun. **55**, 447 (1985).
[25] A. Fernandez, T. Fuji, A. Poppe, A. Furbach, F. Krausz, and A. Apolonski, Opt. Lett. **29**, 1366 (2004).
[26] A. Chong, W. H. Renninger, and F. W. Wise, Opt. Lett. **32**, 2408 (2007).
[27] A. Chong, W. H. Renninger, and F. W. Wise, J. Opt. Soc. Am. B **25**, 140 (2008).
[28] K. Tamura, E. P. Ippen, H. A. Haus, and L. E. Nelson, Opt. Lett. **18**, 1080 (1993).
[29] F. O. Ilday, J. R. Buckley, W. G. Clark, and F. W. Wise, Phys. Rev. Lett. **92**, 213902 (2004).
[30] N. Akhmediev and A. Ankiewicz, in *Spatial Solitons*, edited by S. Trillo and W. E. Toruellas (Springer, Berlin, 2001), pp. 311–342.
[31] N. Akhmediev, J. M. Soto-Crespo, and G. Town, Phys. Rev. E **63**, 056602 (2001).
[32] H. A. Haus, IEEE J. Quantum Electron. **QE-11**, 736 (1975).
[33] S. T. Cundiff, J. M. Soto-Crespo, and N. Akhmediev, Phys. Rev. Lett. **88**, 073903 (2002).
[34] A. Komarov, H. Leblond, and F. Sanchez, Phys. Rev. E **72**, 025604(R) (2005).
[35] G. E. Town and N. Akhmediev, in *Encyclopedia of Modern Optics*, Vol. 2, edited by R. D. Guenther (Academic, New York, 2004), pp. 475–484.
[36] J. M. Soto-Crespo, N. Akhmediev, Ph. Grelu, and F. Belhache, Opt. Lett. **28**, 1757 (2003).
[37] N. N. Akhmediev, V. V. Afanasjev, and J. M. Soto-Crespo, Phys. Rev. E **53**, 1190 (1996).
[38] O. Descalzi and H. R. Brand, Phys. Rev. E **72**, 055202(R) (2005).
[39] O. Descalzi, G. Düring, and E. Tirapegui, Physica A **356**, 66 (2005).
[40] J. M. Soto-Crespo, N. N. Akhmediev, V. V. Afanasjev, and S. Wabnitz, Phys. Rev. E **55**, 4783 (1997).
[41] N. Akhmediev, J. M. Soto-Crespo, and G. Town, Phys. Rev. E **63**, 056602 (2001).
[42] S. T. Cundiff, J. M. Soto-Crespo, and N. Akhmediev, Phys. Rev. Lett. **88**, 073903 (2002).
[43] A. I. Maimistov, J. Exp. Theor. Phys. **77**, 727 (1993).
[44] V. L. Kalashnikov, E. Podivilov, A. Chernykh, and A. Apolonski, Appl. Phys. B: Lasers Opt. **83**, 503 (2006).